

Supplementary Information

Borate decorated anion-immobilized solid polymer electrolyte for dendrite-free, long-life Li metal batteries

Cheng Ma ^a, Yiming Feng ^a, Fangzhou Xing ^a, Lin Zhou ^a, Ying Yang ^a, Qingbing Xia ^b, Liangjun Zhou ^a, Lijun Zhang ^a, Libao Chen ^a, Douglas G. Ivey ^c, Donald R. Sadoway ^d and Weifeng Wei ^{a*}

- a. State Key Laboratory of Powder Metallurgy, Central South University, Changsha, Hunan 410083, People's Republic of China
- b. Institute for Superconducting and Electronic Materials, University of Wollongong, Wollongong, New South Wales, 2522, Australia
- c. Department of Chemical & Materials Engineering, University of Alberta, Edmonton, Alberta, Canada T6G 1H9
- d. Department of Materials Science and Engineering, Massachusetts Institute of Technology, Cambridge, Massachusetts 02139-4307, USA

E-mail: weifengwei@csu.edu.cn

Experimental Section

Synthesis of PEGMA containing boronic ester group (B-PEGMA)^[1]

1 g of 2,5-dimethylhexane-2,5-diol (C₈H₁₈O₂, 99%, Aladdin) and 0.76 mL of trimethyl borate (B(OCH₃)₃, ≥ 99.5%, Aldrich) were dissolved in 10 mL of anhydrous acetonitrile (CH₃CN, 99.8%, Aldrich) under constant stirring and N₂ purging for 1 h at 65 °C. Then 2.45 g of poly(ethylene glycol) methacrylate (PEGMA, Mn=360g mol⁻¹, Aldrich) was injected into the solution and stirred at 65 °C for another 3 h. After the reaction, the product was purified with toluene (anhydrous, Sinopharm Chemical Reagent Co., Ltd), followed by reduced pressure distillation and vacuum drying at 60 °C for 24 h to remove the residual solvent. Finally, the PEGMA containing boronic ester groups was stored in an Ar filled glove box to prevent hydrolyzation.

Synthesis of solid polymer electrolyte (SPE)

P(V-B) electrolytes were synthesized using in-situ polymerization. 0.2 g of bis(trifluoromethanesulfonyl) imide lithium (LiTFSI, 99.95%, Aldrich) and 5 mg azobisisobutyronitrile (AIBN, 98%, Aladdin) were dissolved in 1 g of a mixture consisting of a solution of B-PEGMA and vinylene carbonate (VC, 98%, Aladdin) with different mass ratios. Then, the precursor solution was injected into a cellulose film (Φ18 mm, Nippon Kodoshi Corp., Japan) and sealed in a 2016 coin cell, followed by heating at 60 °C for 24 h and at 80 °C for another 10 h to ensure complete polymerization. The thus-prepared electrolyte was dissolved in dimethylsulfoxide (DMSO, Aladdin) and precipitated in diethyl ether (≥ 99.5%, Sinopharm Chemical reagent Co., Ltd) three times to obtain the purified product. The polymerization conversion rate calculated through dividing the mass of purified product by the mass of electrolyte and was higher than 96%.

Characterization

Structural information of the products was investigated using ¹H nuclear magnetic resonance (NMR) spectroscopy (Avance III 400 MHz Digital NMR spectrometer), Fourier transfer infrared (FTIR) spectroscopy (Nicolet 6700) and powder X-ray diffraction (XRD, Rigaku D/Max-2500) with Cu K α radiation ($\lambda = 1.5406 \text{ \AA}$). Differential scanning calorimetry (DSC) (simultaneous DSC-TGA Q series (SDTQ)-600 TA) and thermogravimetric analysis (TGA, DTA6300) experiments were performed at a heating rate of 10 °C min⁻¹ under N₂ atmosphere. Mechanical properties of the samples were measured using dynamic mechanical analysis (DMA) (Q800, TA instruments) with a sweeping frequency of 0.01–100 Hz. Atomic force microscopy (AFM, Multimode 8) under amplitude modulation-frequency modulation (AM-FM) mode was employed to measure the topography and the Young's modulus of the P(V-B) electrolyte. Scanning electron microscopy (SEM, Nova Nano SEM 230) was utilized to characterize the surface and cross-section morphologies. X-ray photoelectron spectroscopy (XPS) was conducted on a Thermo Scientific ESCALab 250Xi to detect the surface chemistry of the Li-metal anode.

Electrochemistry

Ionic conductivity was measured using electrochemical impedance spectroscopy (EIS) with symmetric SS (stainless steel)/SPE/SS cells in the frequency range of 0.1 Hz to 100 kHz with a 10 mV amplitude. Conductivity values were calculated on the basis of the electrolyte resistance (R_b), the thickness of the electrolyte film (L) and the electrode area (A), according to Equation (1):

$$\sigma = L/R_b A \quad (1)$$

The Nyquist plots were modeled and the activation energy, E_a , for Li^+ conduction was calculated from the Arrhenius equation:

$$\sigma = A \exp(-E_a/k_b T) \quad (2)$$

where A represents the frequency factor, k_b is Boltzmann's constant and T is the absolute temperature.

Li^+ transference numbers (t^+) were evaluated by combining DC polarization/AC impedance in symmetric Li/SPE/Li cells based on the following equation:

$$t^+ = \frac{I_{ss}(\Delta V - I_0 R_0)}{I_0(\Delta V - I_{ss} R_{ss})} \quad (3)$$

where ΔV represents the polarization voltage applied, I_0 and R_0 are the initial current and interfacial resistance and I_{ss} and R_{ss} are the steady state current and interfacial resistance, respectively.

Cyclic voltammetry was employed to determine the electrochemical stability of the P(V-B) electrolyte in SS/SPE/Li coin cells, which included a negative scan from 2.5 V to -0.5 V and a positive scan from 2.5 V to 5 V at a rate of 5 mV s⁻¹.

Battery test

For LiFePO_4 (LFP)/Li and $\text{LiNi}_{0.6}\text{Co}_{0.2}\text{Mn}_{0.2}\text{O}_2$ (NCM-622)/Li coin cells, 80% LFP/NCM-622 (MTI Kejing Group) powders, 10% carbon black (Yiborui Chemical Industry Company, Tianjin, China), and 10% polyvinylidene fluoride binder (PVDF, Arkema Inc) were fully mixed in N-methyl-2-pyrrolidone (NMP, Aladdin) and the resultant slurry was coated onto Al foil and dried in a vacuum oven at 110 °C for 12 h to remove the residual NMP. The typical active material loading was about 1.5 mg cm⁻².

For the flexible LFP/SPE/Li full cell, inks containing the active materials of LFP, poly(vinylidene fluoride-co-hexafluoropropylene) (PVDF-HFP, Mn = ~130,000 g mol⁻¹, Aldrich) and carbon black dispersed in NMP were printed on a glass plate with a 3D printer (Fisnar F4200N), followed by a water coagulation bath. Then the wet electrode was peeled off and transferred to a freeze dryer (Christ, Alpa 1-2 LDplus) to obtain the final flexible electrode with a size of 3.5 cm × 1.8 cm. For liquid electrolyte based LFP/Li and Li/Li cells, the 1M LiPF_6 (> 97.0%, Aladdin) in 1:1:1 (by volume) ethylene carbonate/dimethyl carbonate/diethyl carbonate (anhydrous, Aladdin) was prepared in

laboratory and used after further removing the residual water by molecular sieves. All coin cells and flexible full cells were assembled in an Ar-filled glove box and the charge–discharge tests were carried out using a battery testing system (LANHE CT2001A, Wuhan LAND Electronics Co.).

Density functional theory (DFT) calculations

The Gaussian 16 package^[2] was used to carry out all the DFT calculations based on the Lee-Yang-Parr correlation functional (B3LYP). Geometry optimizations were performed with a full electron 6-31+G(d,p) basis set for the TFSl and polymer molecule, and 6-311+G(d,p) for the absorbed molecules along with the basis set superposition error (BSSE) correction. Natural band orbital (NBO) analyses were also performed through single-point calculations to further investigate the interaction between Li⁺ and the carbonate and ether oxygen groups.

Simulation of Li⁺ concentration distribution

Python software combined with the separation variable method was employed to investigate the distribution of Li⁺, and both electric field and diffusion flow were taken into account in the simulations. Onsager's theory and the diffusivity equations listed below were coupled to conduct the simulation.

$$J_i = -L_{ii}\nabla\eta_i = -M_iC_i(\nabla\mu_i + zF\nabla E) \quad (4)$$

$$J_i = -D_i\nabla C_i + v_iC_i\nabla E \quad (5)$$

$$\frac{\partial C_i}{\partial t} = -\nabla J_i \quad (6)$$

where η_i is the electrochemical potential energy of species i , L_{ii} is the transport coefficient of species i , μ_i is the chemical potential of species i , z is the ionic charge number, F is the Faraday constant, E is the electric potential, M_i is the atomic mobility parameter of species i , C_i is the concentration of species, D_i is the diffusion coefficient of species i , v_i is the ionic mobility of species i and J_i is the flux vector of species i . Each simulation was performed in a unit volume and the distance between two electrodes and the Li deposition/dissolution rate J_{Li} were set as 80 μm and $10^{-4} \text{ mol m}^{-2} \text{ s}^{-1}$, respectively.

The mobility of Li⁺, v_{Li} , and the diffusion coefficient of Li⁺, D_{Li} , were calculated using Equations (7) and (8) and the values are listed in the table S4 according to the percentage of immobilized anions

$$\sigma = C_i e v_i \quad (7)$$

$$D_i = \frac{v_i}{zF}RT \quad (8)$$

where σ is the ionic conductivity, e is the carrier charge, R is the gas constant, and T is the absolute temperature.

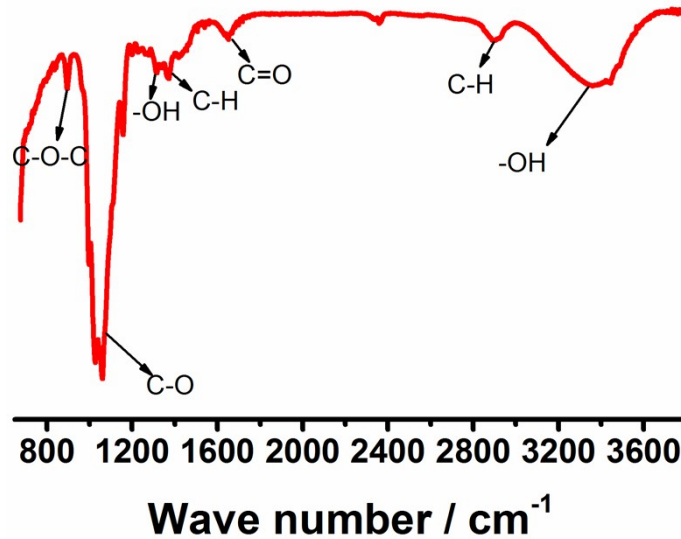


Fig. S1 Fourier transform infrared (FTIR) spectrum of cellulose membrane.

Fig. S1 demonstrates that rich oxygen functional groups exist in the structure of cellulose membrane, with peaks at 3400 cm⁻¹ and 1321 cm⁻¹ for -OH stretching and bending vibrations, 1650 cm⁻¹ for the C=O stretching vibration, as well as at 1064 cm⁻¹ and 895 cm⁻¹ for C-O and cyclical C-O-C stretching vibrations.



Fig. S2 Optical photograph of P(V-B) electrolyte with different weight fractions of B-PEGMA (0 wt%, 5 wt%, 10 wt%, 20 wt% and 30 wt%, from left to right).

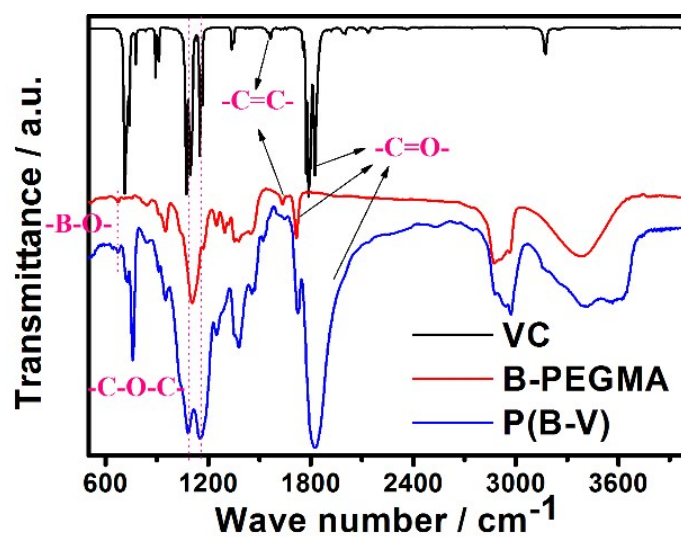


Fig. S3 FTIR spectra of VC, B-PEGMA and as synthesized P(V-B).

Fourier transform infrared spectroscopy (FTIR) in Fig. S3 reveal that the intensity of vinyl peaks at 1565cm^{-1} for VC and 1635cm^{-1} for B-PEGMA significantly decreases after polymerization, while other characteristic peaks related to the $-\text{C}=\text{O}-$, $-\text{C}-\text{O}-$ and $-\text{B}-\text{O}-$ bonds still exist.

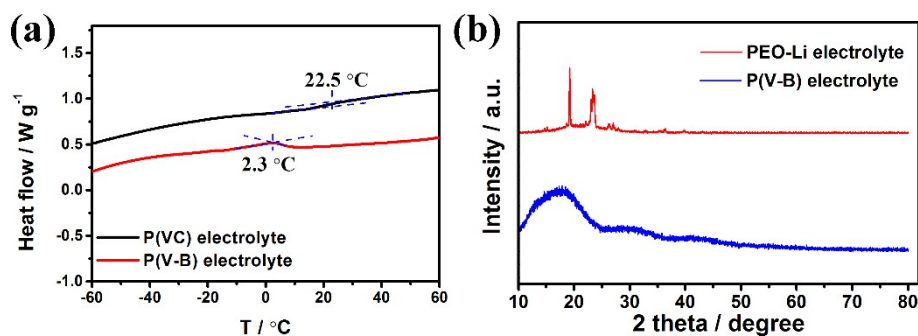


Fig. S4 (a) DSC curves of P(V-C) and P(V-B) electrolyte. (b) XRD patterns of polyethylene oxide (PEO)-Li and the P(V-B) electrolyte.

The DSC curve for the P(V-B) electrolyte (Fig. S4a) shows a small peak at 2.3 °C, instead of a steep slope, which is ascribed to stress relaxation of chain segments during the glass transition process.

The X-ray diffraction (XRD) pattern (Fig. S4b) consists of only one broad peak centered at 17.4°, which exposes the amorphous nature of the P(V-B) electrolyte, because the natural semi-crystalline structure of EO groups is disrupted by VC segments.

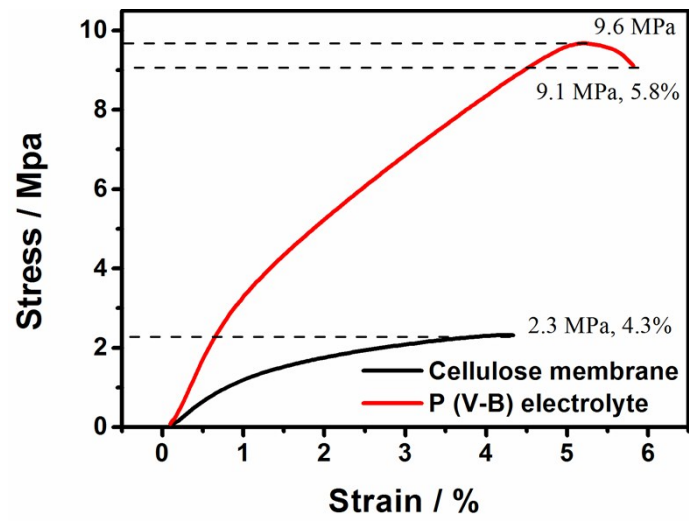


Fig. S5 Stress-strain curves of cellulose membrane and P(V-B) electrolyte.

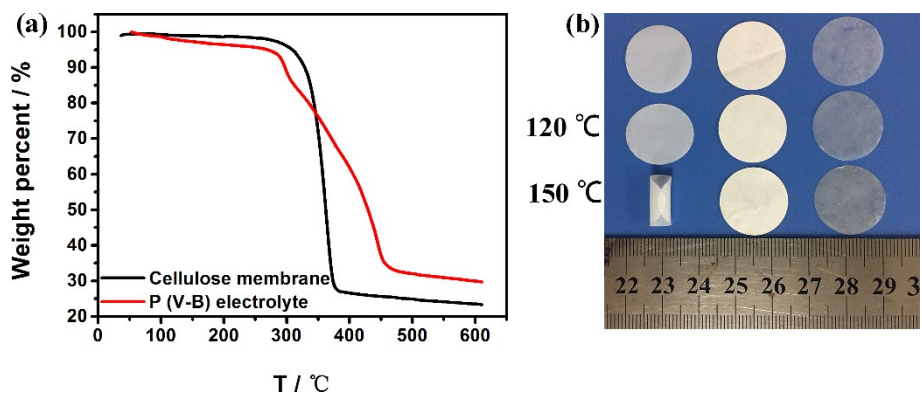


Fig.S6 (a) TG curves of cellulose membrane and P(V-B) electrolyte. (b) Optical photograph of Celgard PP separator, cellulose membrane and P(V-B) electrolyte (from left to right) before and after heating at 120 and 150 °C.

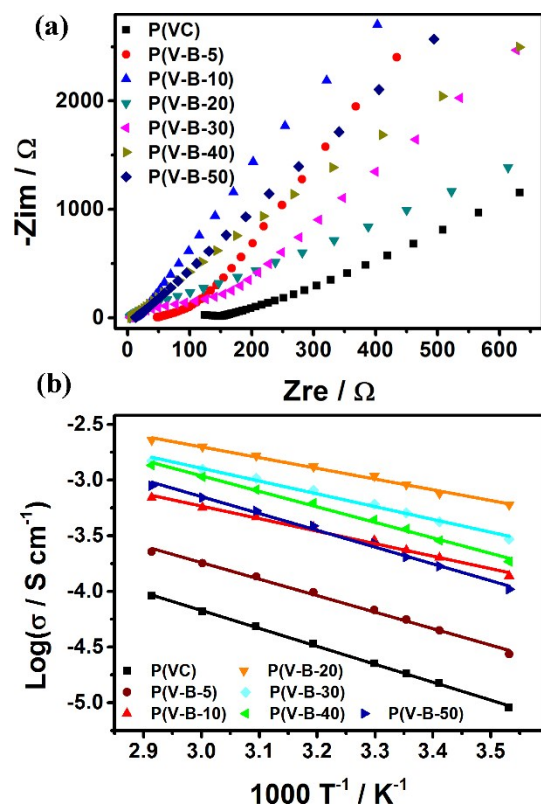


Fig. S7 (a) EIS measurements at 25 °C and (b) Arrhenius plots at temperatures from 10 to 70 °C for P(V-B) electrolyte with different weight fractions of B-PEGMA.

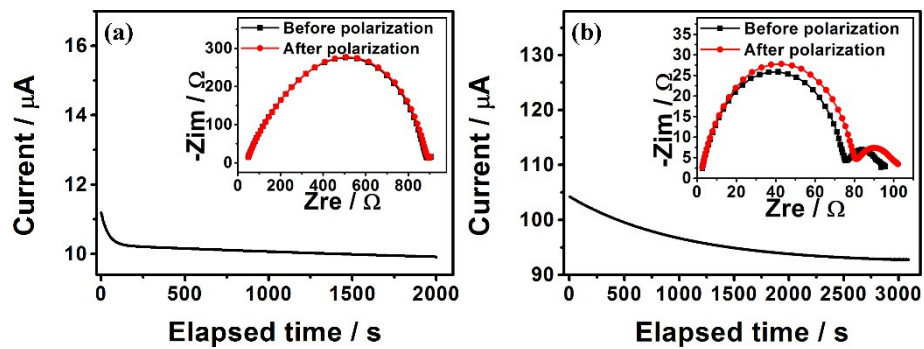


Fig. S8 Current-time plots with AC impedance spectra before and after polarization (inset) of symmetric Li cells with (a) P(VC) and (b) liquid electrolyte.

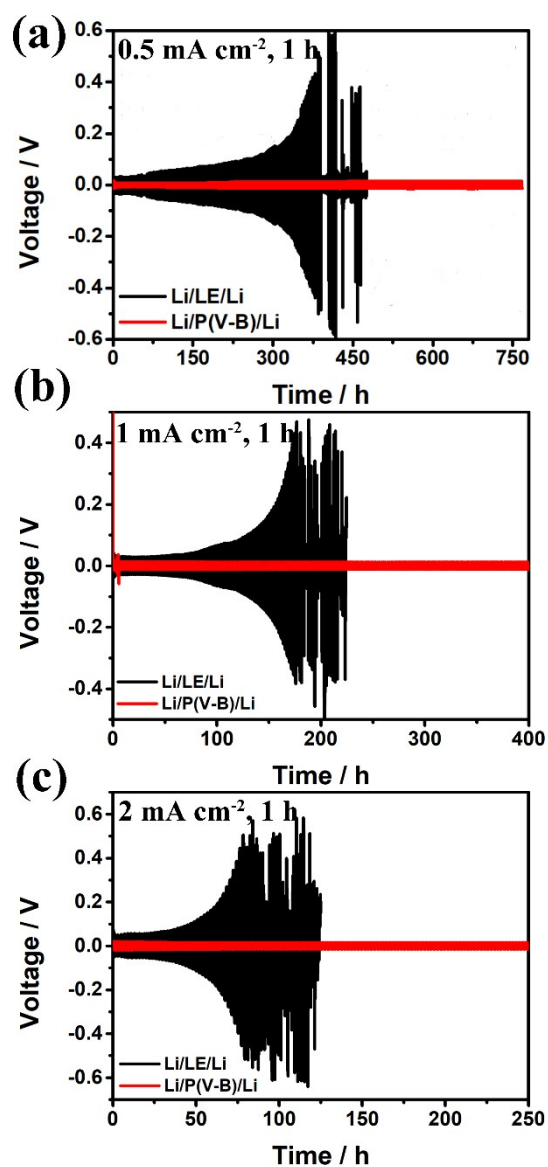


Fig. S9 Voltage profiles of Li plating/stripping in symmetric Li cells containing LE (black) and P(V-B) electrolyte (red) at current densities of (a) 0.5, (b) 1 and (c) 2 mA cm^{-2} for 1 h, respectively.

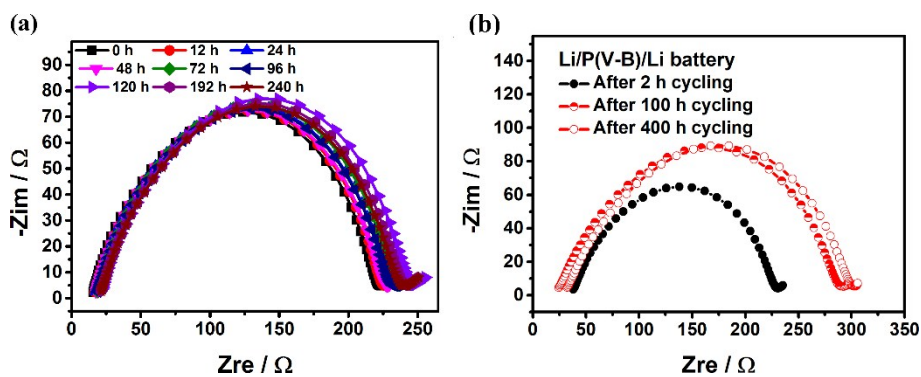


Fig. S10 EIS spectra of symmetric Li cell with P(V-B) electrolyte for (a) different aging times and (b) different cycling times (1 mA cm^{-2} , 1h) at $30 \text{ }^\circ\text{C}$.

The interfacial stability between the P(V-B) electrolyte and lithium metal was also probed using Nyquist profiles of the symmetric Li cell. It can be seen that the interfacial resistance is about $210 \text{ } \Omega$, which remains stable for a period of 240 h and slightly increase to $270 \text{ } \Omega$ after 400 h cycling at $30 \text{ }^\circ\text{C}$.

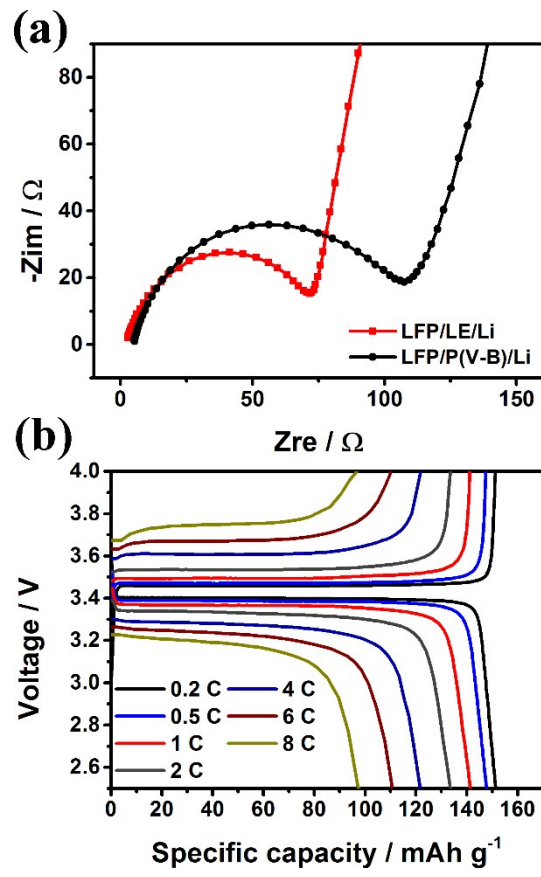


Fig. S11 (a) EIS spectra of LFP/Li batteries with LE and the P(V-B) electrolyte. (b) charge-discharge curves at various C-rates of an LFP/Li battery containing the P(V-B) electrolyte at 30 °C.

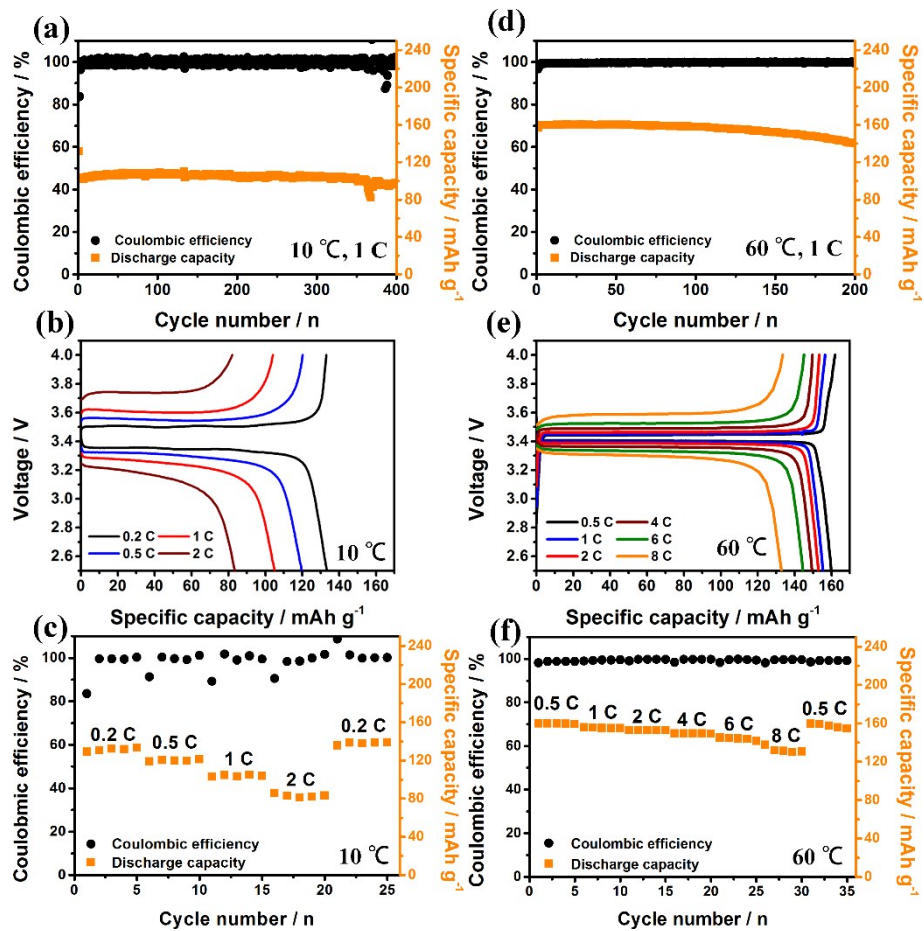


Fig. S12 (a, d) Cycling performance, (b, e) charge and discharge curves at various rates and (c, f) rate capacities of LFP/Li batteries with P(V-B) electrolyte at 10 °C (a-c) and 60 °C (d-f).

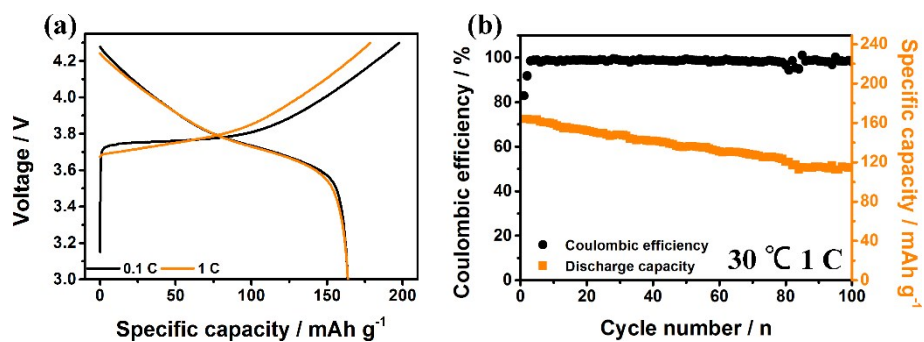


Fig. S13 (a) Charge/discharge potential curves and (b) cycling performance of LiNi_{0.6}Co_{0.2}Mn_{0.2}O₂/P(V-B) electrolyte/Li metal battery at 30 °C and 1 C.

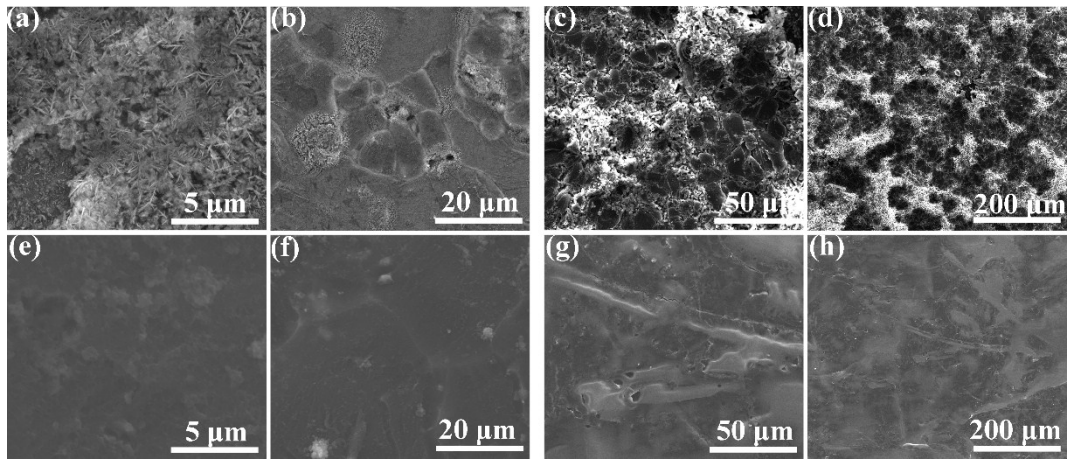


Fig. S14 SEM SE images of Li anodes from LFP/Li metal batteries for 50 (a, b, e, f) and 100 cycles (c, d, g, h) with LE (a-d) and P(V-B) electrolyte (e-h), respectively.

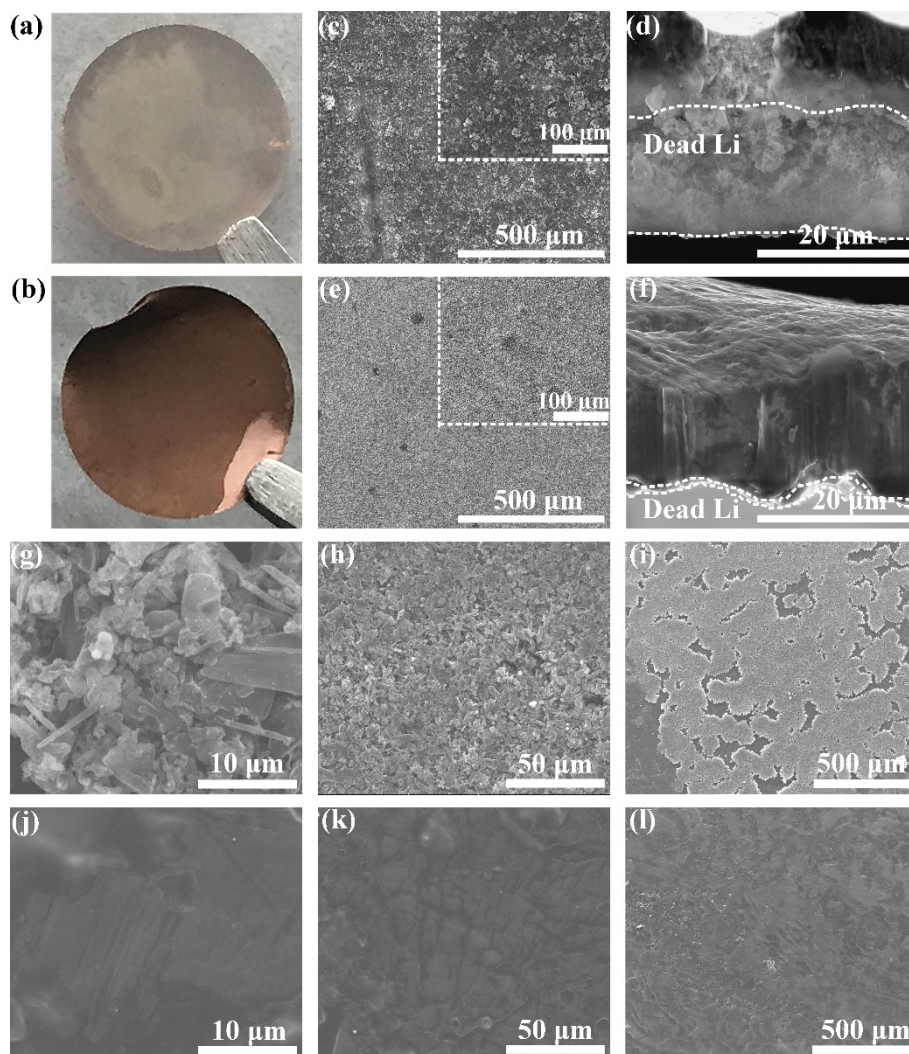


Fig. S15 Optical photographs of Cu foil (a, b) and SEM SE images of Cu foil (c-f) and Li anode (g-l) for LE (a, c, d, g-i) and P(V-B) electrolyte (b, e, f, j-l) based Li/Cu asymmetric cells after 10 charge cycles with a plating/stripping capacity of 0.5 mAh cm^{-2} at 0.5 mA cm^{-2} .

Li/Cu asymmetric cells were assembled to further evaluate Li plating/stripping behavior on the electrolyte/electrode interface. After 10 cycles, the optical photographs of Cu foil reveal massive and silver Li deposits for the Li/LE/Cu cell (Fig. S15a). In contrast, the P(V-B) electrolyte-based cell results in a slight and dark gray Li deposits on the Cu foil (Fig. S15b), which reveals a higher Li^+ utilization and more reversible Li plating/stripping behavior. In addition, the morphologies of the Li deposits on the Cu substrates and Li anodes were also recorded. The LE samples have an uneven surface composed of larger cluster-like dead Li with a thickness of about $20 \mu\text{m}$ on the Cu foil (Fig. S15c, d). Sharp and rigid dendrites are visible on the surface of the Li anode as well (Fig. S15g-i). The P(V-B) electrolyte enables the formation of a uniform and dense plated Li layer without a conspicuous dead Li layer on the substrate (Fig. S15e, f), as well as dendrite-free morphology for the Li metal (Fig. S15j-l).

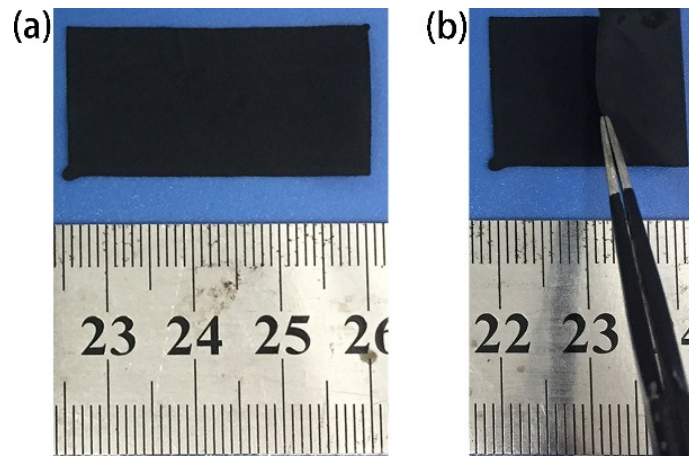


Fig. S16 Optical photographs of flexible LFP cathode.

Table S1 Comparative data on the electrochemical properties and battery performances of SPE from recent publications.

Samples (physical state)	$\sigma \times 10^4$ at ambient temperature (S cm ⁻¹)	t_{Li^+}	Mechanical properties		Cycling stability (battery-C rate- temperature-cycles- capacity retention)	ref
			Tensile strength (MPa)	Young's modulus (Gpa)		
This work (solid-state)	9.11	0.68	9.6	2.41	LFP/Li-1 C-30 °C-600th 93.3% NCM622/Li-1 C-30 °C- 100th-75%	
PPC-LLZTO (solid-state)	5.2	0.75	6.8	\	LFP/Li-0.5 C-20 °C- 200 th -95%	[3]
PVCA (solid-state)	0.22	0.57	\	\	LCO/Li-0.1 C-50 °C- 150 th -84.2%	[4]
IPN-PEA (quasi-solid-state)	2.2	0.65	\	12	LFP/Li-1 C-25 °C-200 th - 85%	[5]
PEO/SiO ₂ aerogel (solid-state)	6			0.43	LFP/Li-0.5 C-18 °C- 200 th ->80%	[6]
PEC/LiMNT (quasi-solid-stste)	3.5	0.83	5.3	\	LFP/3DLi-0.5 C-25 °C- 200 th -91.9%	[7]
PEO/CMOF (solid-state)	0.31	0.72	9.7		Al ₂ O ₃ @NCM523/3DLi- 0.2 C-25 °C-100 th -92%	[8]
PVDF/LLZTO (solid-state)	5		5.92	0.03	LFP/Li-1 C-60 °C-300 th - 85.4%	[9]
PEO/VAVS (solid-state)	1.89	0.47		0.035	LFMP/Li-0.1 C-60° C- 100 th -81.2%	[10]

PPC: poly(propylene carbonate); LLZTO: Li_{6.75}La₃Zr_{1.75}Ta_{0.25}O₁₂; PVCA: Poly (Vinylene Carbonate); IPN-PEA: interpenetrating polymer network –poly(ethyl acrylate); LiMNT: lithium montmorillonite; CMOF: cationic metal-organic framework; VAVS: vertically aligned vermiculite sheets.

Table S2. Ionic conductivity and other parameters for P(V-B) electrolytes with different weight fractions of B-PEGMA.

	σ (S cm ⁻¹)	A (s cm ⁻¹ k ^{1/2})	E _a (kJ mol ⁻¹)
P(V-C)	1.83 × 10 ⁻⁵	1.95	13.40
P(V-B-5)	5.57 × 10 ⁻⁵	2.03	12.33
P(V-B-10)	2.34 × 10 ⁻⁴	1.15	9.35
P(V-B-20)	9.11 × 10⁻⁴	1.20	8.00
P(V-B-30)	5.08 × 10 ⁻⁴	1.74	9.56
P(V-B-40)	3.63 × 10 ⁻⁴	3.39	11.59
P(V-B-50)	2.03 × 10 ⁻⁴	3.99	12.56

Table S3. Lithium ion transference number for liquid, P(VC) and the P(V-B) electrolytes.

	R_0 / Ω	R_{ss} / Ω	$I_0 / \mu A$	$I_{ss} / \mu A$	t_{Li^+}
Liquid electrolyte	94.41	101.92	104.23	92.70	0.26
P(VC) electrolyte	849.3	852.7	10.92	9.94	0.43
P(V-B) electrolyte	244.85	289.65	29.31	23.21	0.68

Table S4. Diffusion and mobility data calculated from Equations (7) and (8).

Immobilized anions (%)	C_{Li} (mol m ⁻³)	C_A (mol m ⁻³)	v_{Li} (m ² V ⁻¹ s ⁻¹)	D_{Li} (m ² s ⁻¹)
0	1000	1000	4.72×10^{-10}	1.21×10^{-11}
25	1000	750	5.39×10^{-10}	1.38×10^{-11}
50	1000	500	6.29×10^{-10}	1.61×10^{-11}
75	1000	250	7.55×10^{-10}	1.94×10^{-11}
100	1000	0	9.44×10^{-10}	2.43×10^{-11}

Notes and references

- [1] J. F. Zhang, C. Ma, H. Hou, X. F., Li, L. B. Chen, D. G. Ivey and W. F. Wei, *J. Membr. Sci.* 2018, **552**, 107-114.
- [2] M.J. Frisch, G.W. Trucks, H.B. Schlegel, G.E. Scuseria, M.A. Robb, J.R. Cheeseman, G. Scalmani, V. Barone, B. Mennucci, G.A. Petersson, H. Nakatsuji, M. Caricato, X. Li, H.P. Hratchian, A.F. Izmaylov, J. Bloino, G. Zheng, J.L. Sonnenberg, M. Hada, M. Ehara, K. Toyota, R. Fukuda, J. Hasegawa, M. Ishida, T. Nakajima, Y. Honda, O. Kitao, H. Nakai, T. Vreven, J.A. Montgomery Jr., J.E. Peralta, F. Ogliaro, M. Bearpark, J.J. Heyd, E. Brothers, K.N. Kudin, V.N. Staroverov, T. Keith, R. Kobayashi, J. Normand, K. Raghavachari, A. Rendell, J.C. Burant, S.S. Iyengar, J. Tomasi, M. Cossi, N. Rega, J.M. Millam, M. Klene, J.E. Knox, J.B. Cross, V. Bakken, C. Adamo, J. Jaramillo, R. Gomperts, R.E. Stratmann, O. Yazyev, A.J. Austin, R. Cammi, C. Pomelli, J.W. Ochterski, R.L. Martin, K. Morokuma, V.G. Zakrzewski, G.A. Voth, P. Salvador, J.J. Dannenberg, S. Dapprich, A.D. Daniels, O. Farkas, J.B. Foresman, J.V. Ortiz, J. Cioslowski, D.J. Fox, Gaussian 16, Revision C.01, Gaussian, Inc., Wallingford CT, 2013.
- [3] J. J. Zhang, X. Zang, H. J. Wen, T. T. Dong, J. C. Chai, Y. Li, B. B. Chen, J. W. Zhao, S. M. Dong and J. Ma, *J. Mater. Chem. A*, 2017, **5**, 4940-4948.
- [4] J. C. Chai, Z. H. Liu, J. Ma, J. Wang, X. C. Liu, H. S. Liu, J. J. Zhang, G. L. Cui and L. Q. Chen, *Adv. Sci.*, 2017, **4**, 1600377
- [5] X. X. Zeng, Y. X. Yin, N. W. Li, W. C. Du, Y. G. Guo and L. J. Wan, *J. Am. Chem. Soc.*, 2016, **138**, 15825-15828.
- [6] D. C. Lin, P. Y. Yuen, Y. Y. Liu, W. Liu, N. Liu, R. H. Dauskardt and Y. Cui, *Adv. Mater.*, 2018, **30**, 1802661.
- [7] L. Chen, W. X. Li, L. Z. Fan, C. W. Nan and Q. Zhang, *Adv. Funct. Mater.*, 2019, **0**, 1901047.
- [8] H. Y. Huo, B. Wu, T. Zhang, X. S. Zheng, L. Ge, T. W. Xu, X. X. Guo and X. L. Sun, *Energy Storage Mater.*, 2019, **18**, 59-67..
- [9] X. Zhang, T. Liu, S. F. Zhang, X. Huang, B. Q. Xu, Y. H. Lin, B. Xu, L. L. Li, C. W. Nan and Y. Shen, *J. Am. Chem. Soc.*, 2017, **139**, 13779-13785.
- [10] W. J. Tang, S. Tang, X. Z. Guan, X. Y. Zhang, Q. Xiang and J. Y. Luo, *Adv. Funct. Mater.*, 2019, **29**, 1900648.